Engineering a Pt nanoparticles-modified nanoporous boron-doped diamond electrode for efficient electrochemical ozone production

Zijian Tang [a,1], Sen Ming [a,1], Xiang Wang [a], Jie Wang [a], Junkui Zhu [a], Zejun Deng [a,*], Kechao Zhou [b], Li Ma [b,*], Qiuping Wei

[a] *School of Materials Science and Engineering, Central South University, Changsha 410083, China*

[b] *State Key Laboratory of Powder Metallurgy, Central South University, Changsha 410083, China*

[*]Corresponding authors: zejun.deng@csu.edu.cn (**Dr. Z. Deng**); marycsupm@csu.edu.cn (**Dr. L. Ma**).

Table of Contents

1. The cross-section morphology of the as-prepared Si/BDD electrodes.

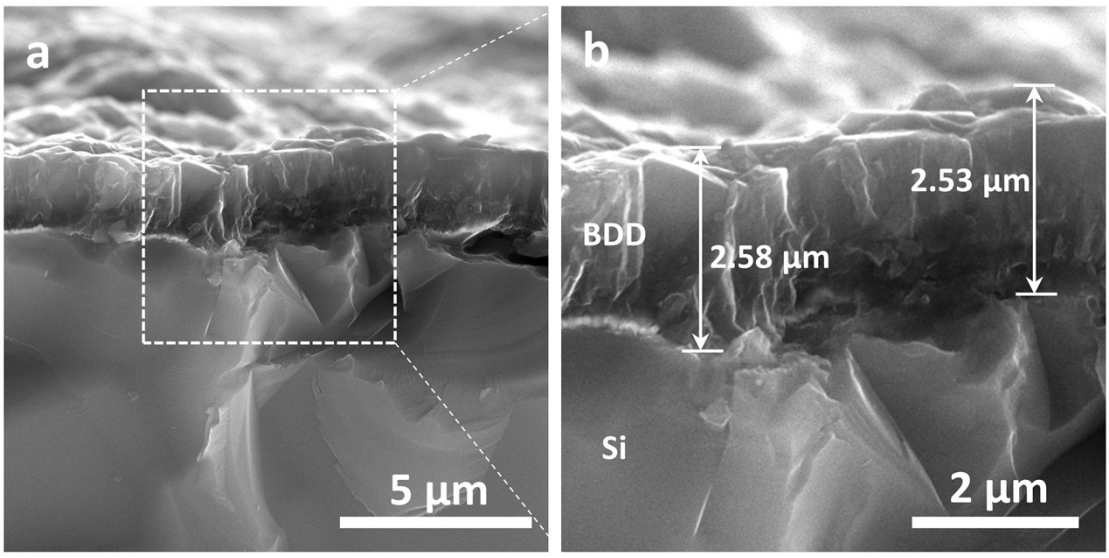

Fig. S1. SEM images showing the cross-section of BDD at (a) low and (b) high magnifications. The thickness of the BDD ranges from approximately 2.5 to 2.6 µm.

2. SEM images of Pt/BDD electrodes.

During electrodeposition, platinum nanoparticles were easily agglomerated. When the deposition time was 30 s, the Pt nanoparticles were more uniform. When the deposition time exceeded 70 s, the Pt nanoparticles appeared to be agglomerated. Platinum nanoparticles tended to nucleate and grow at etched holes and grain boundaries.

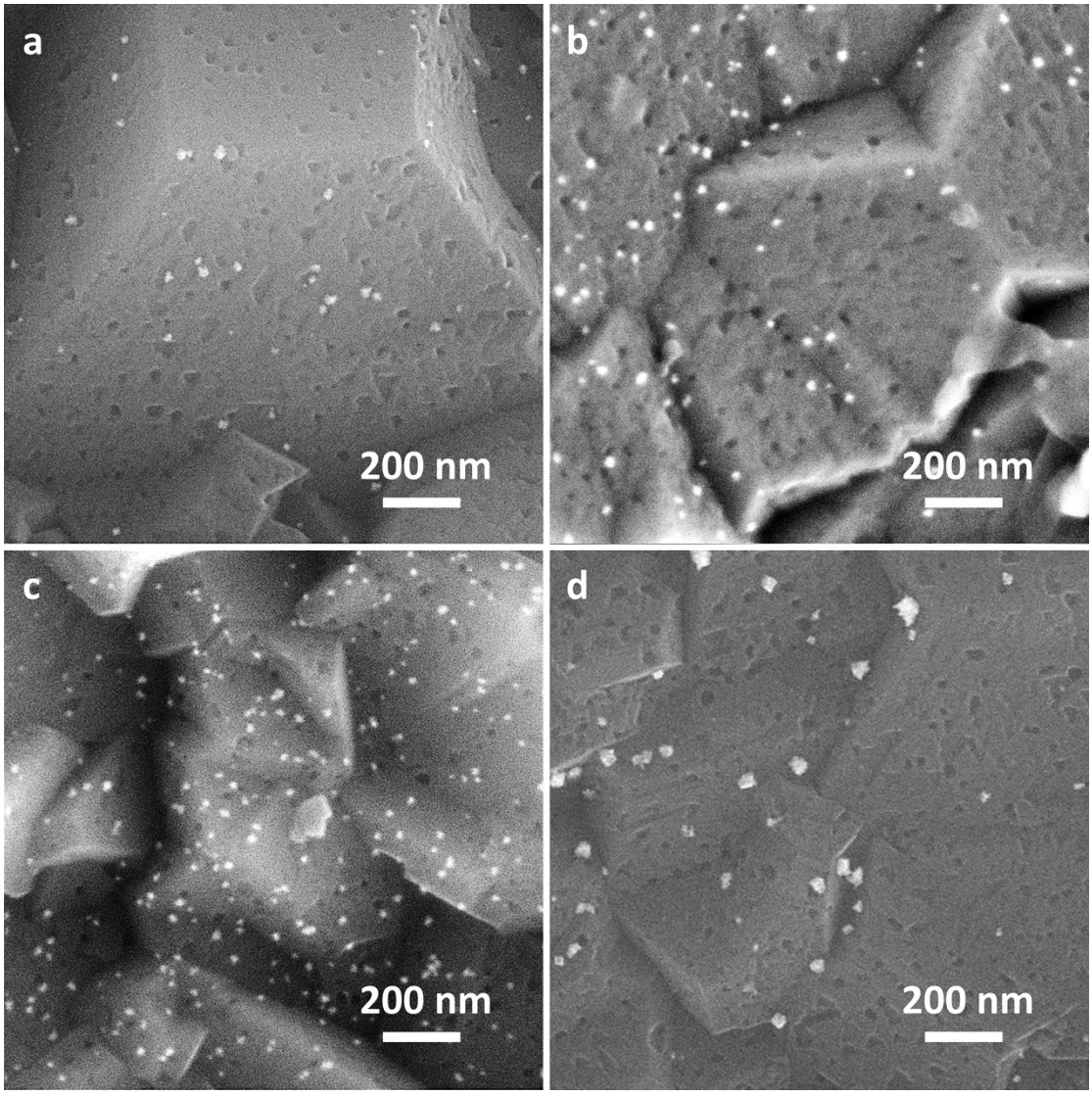

Fig. S2. SEM images of Pt/BDD with different parameters. (a) Pt/PBDD-1 (10 s), (b) Pt/PBDD-2 (30 s), (c) Pt/PBDD-3 (50 s) and (d) Pt/PBDD-4 (70 s).

3. The particles size distribution of Pt/PBDD.

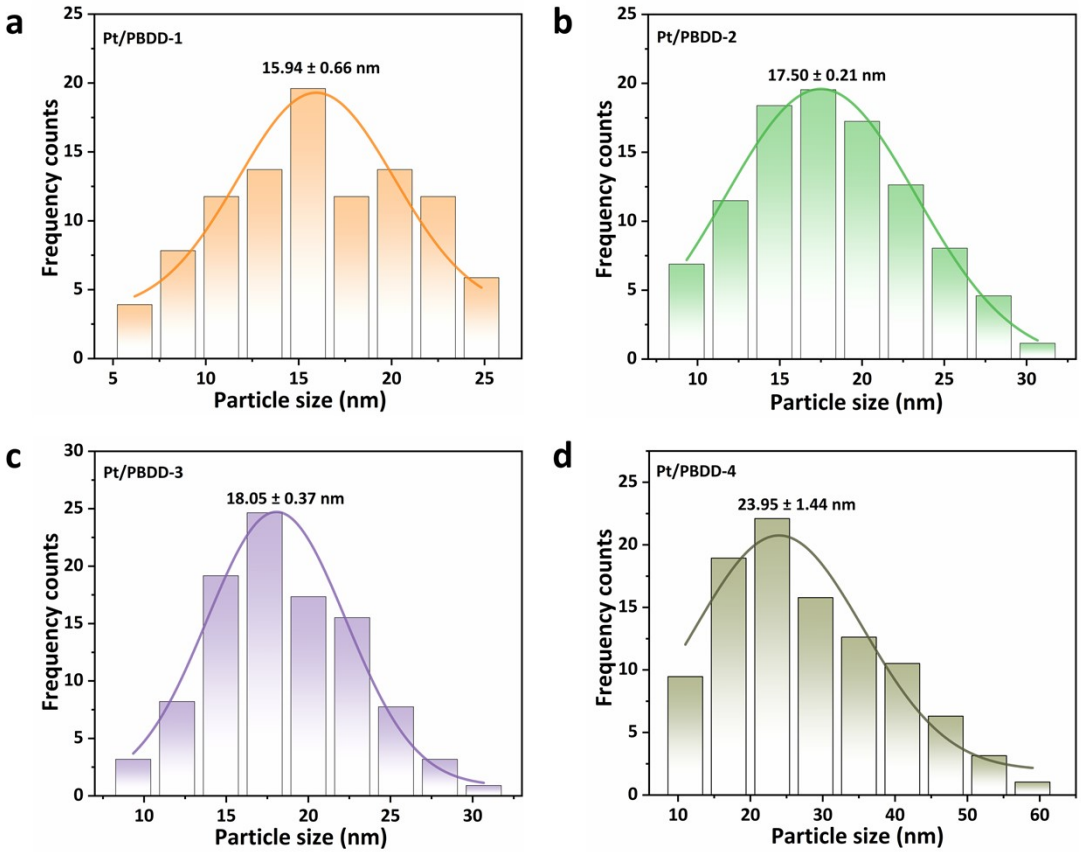

Fig. S3. The particles distribution of Pt/BDD with different parameters. (a) Pt/PBDD-1 (10 s), (b) Pt/PBDD-2 (30 s), (c) Pt/PBDD-3 (50 s) and (d) Pt/PBDD-4 (70 s).

4. The composition of BDD electrodes.

Table. S1. Proportion of elements in diamond electrodes (XPS).

Atomic %	C	O	Pt
RBDD	94.29	5.71	0
PBDD	85.91	14.09	0
Pt/PBDD-1	88.37	11.59	0.04
Pt/PBDD-2	85.99	13.95	0.06
Pt/PBDD-3	87.10	12.80	0.10
Pt/PBDD-4	85.72	14.11	0.17

5. The XPS annlysis of BDD electrodes.

Table. S2. Summary of functional groups for RBDD obtained from XPS analysis.

C 1s	Binding energy (eV)	Peak area ratio (%)
C-C	284.8	55.2
C=C	283.0	1.5
C-H	283.9	5.8
C-O	285.5	20.1
C=O	286.1	13.3
COOH	288.0	4.1
O 1s	Binding energy (eV)	Peak area ratio (%)
Oads	532.7	100

Table. S3. Summary of functional groups for Pt/PBDD obtained from XPS analysis.

C 1s	Binding energy (eV)	Peak area ratio (%)
C-C	284.8	52.8
C=C	283.1	2.5
C-H	284.1	6.0
C-O	285.5	22.0
C=O	286.5	12.5
COOH	288.5	4.2
O 1s	Binding energy (eV)	Peak area ratio (%)
Oads	532.4	100
Pt 4f	Binding energy (eV)	Peak area ratio (%)
Pt2+	73.0 / 76.3	57.4
Pt0	71.4 / 74.8	42.6

6. The electrochemically active area of BDD electrodes.

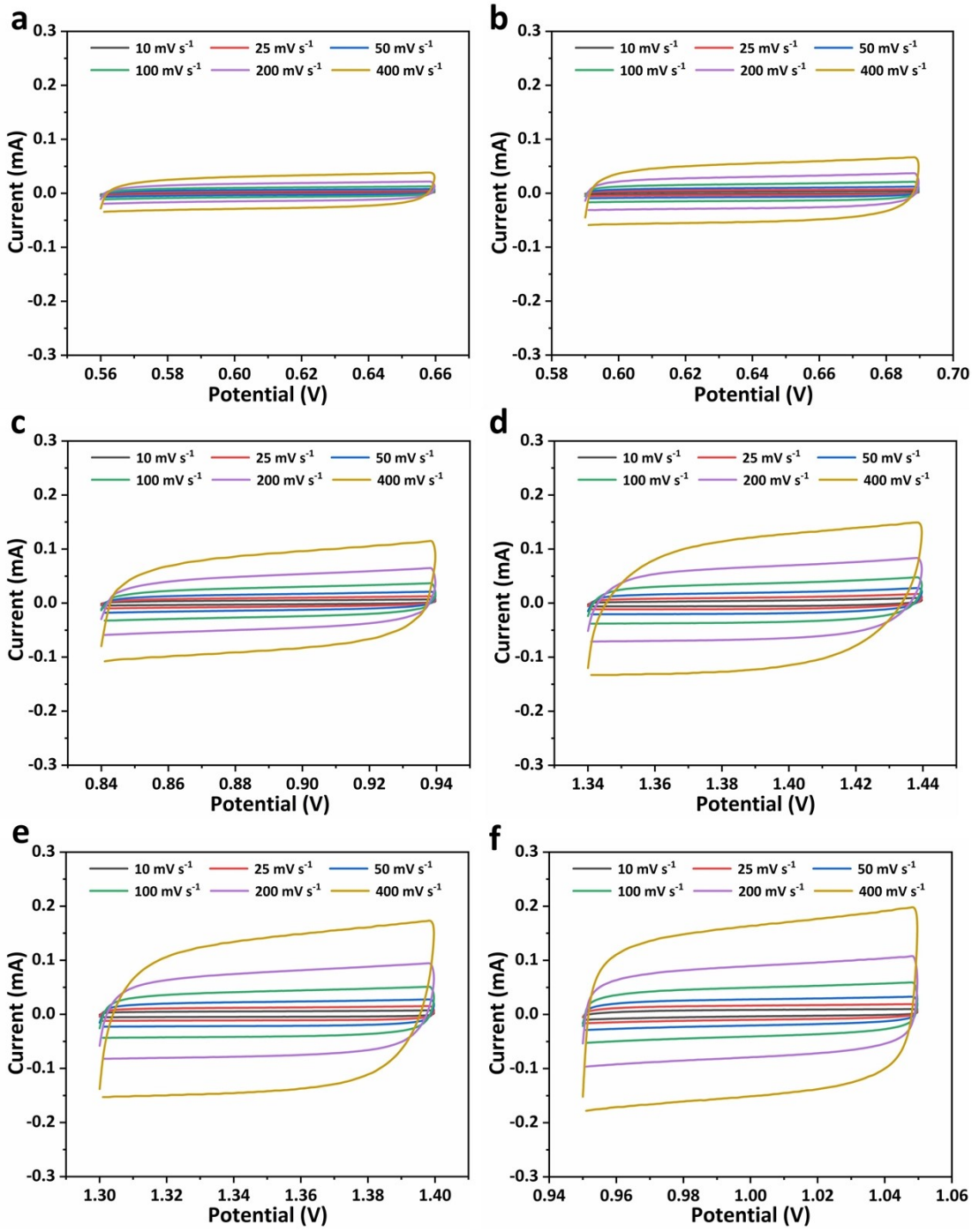

Fig. S4. Cyclic voltammograms measured of (a) RBDD, (b) PBDD, (c) Pt/PBDD-1, (d) Pt/PBDD-2, (e) Pt/PBDD-3 and (f) Pt/PBDD-4 at a potential window of 0.1 V centered at the open circuit potential (OCP). The scan rates are from 10 to 400 mV s^{-1}, and the solution is 0.5 M H_2SO_4.

7. The qualitative characterization of ozonated water.

The higher the concentration of ozonated water, the redder the colour of the detection solution.

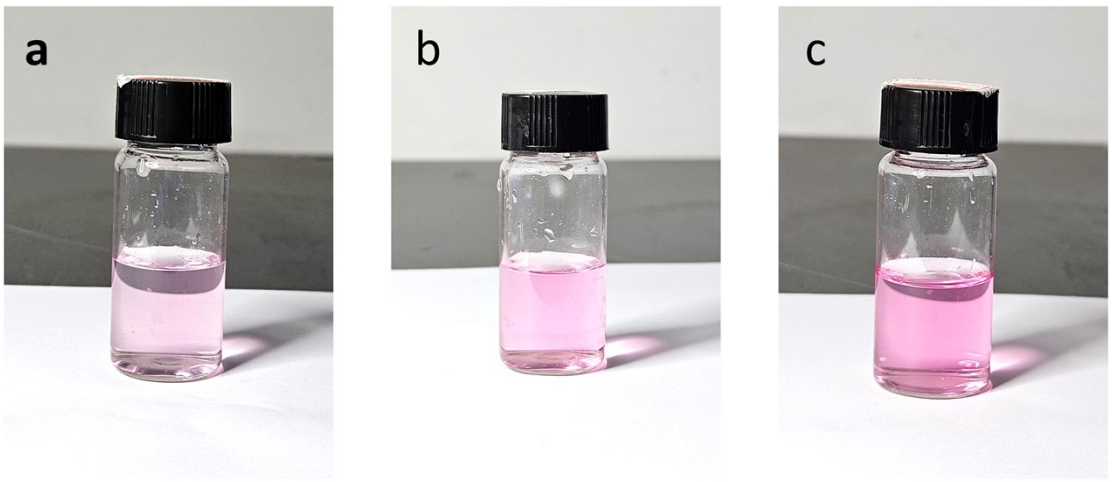

Fig. S5. Ozone Detection Powder giving a qualitative comparison of ozonated water of (a) RBDD, (b) PBDD and (c) Pt/PBDD-2 at the current density of 100 mA cm^{-2}.

8. The qualitative characterization of ozone gas.

The higher the concentration of ozone gas, the purpler the colour of the test paper.

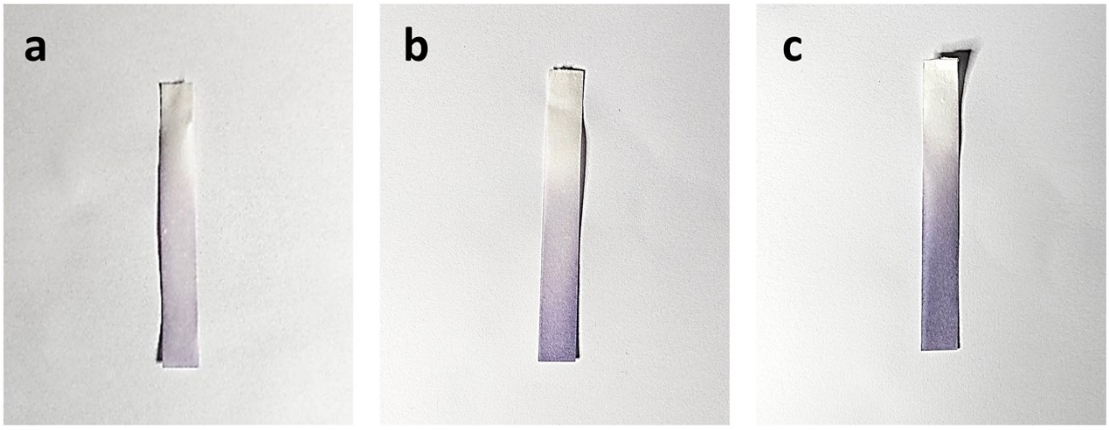

Fig. S6. Wetted starch potassium iodide test paper giving a qualitative comparison of ozone gas of (a) RBDD, (b) PBDD and (c) Pt/PBDD-2 at the current density of 100 mA cm^{-2}.

9. The standard curve of Methylene blue.

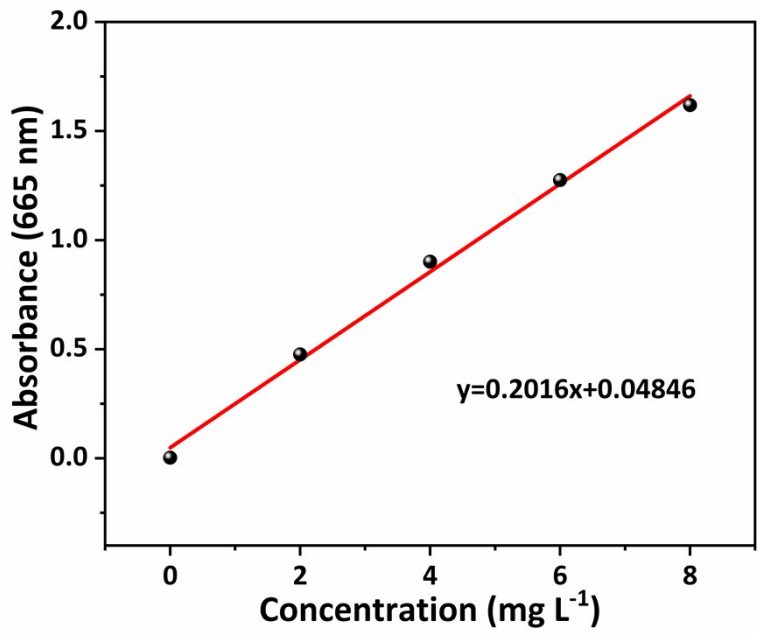

Fig. S7. The standard curve of MB by UV-Vis spectrophotometer.

10. Reported current efficiency for EOP on different anodes.

Table. S4. Reported current efficiency for EOP on different anodes

Anode	Electrolyte	Current density ($mA\ cm^{-2}$)	Faradaic efficiency (%)	Ref.
3D-porous *β*-PbO_2	0.5 M H_2SO_4	100	14.73	[1]
PtCo/Co_2B	saturated K_2SO_4	50	9.09	[2]
Nd-Ni-Sb-SnO_2	0.5 M H_2SO_4	250	33.6	[3]
Ni/Sb-SnO_2@3D-PTi	0.5 M H_2SO_4	20	28	[4]
TaO/TaN-700	saturated K_2SO_4	50	14	[5]
Pt_1/BND	saturated K_2SO_4	50	12.54	[6]
PVP-48	PEM	830	11.9	[7]
Pb_2O_3@Bi_2O_3-tube	saturated K_2SO_4	50	11.29	[8]
Pt/TiN NRs-1	saturated K_2SO_4	50	13	[9]
$Bi_6Pb_2O_X$	saturated K_2SO_4	75	13.5	[10]
PbO_2 nanorod	PEM	4 V	14	[11]
SnO-1	saturated K_2SO_4	50	22.0	[12]
cubic-Pb_3O_4@SiO_2	PEM	1000	21.2	[13]
2D ND-1100	saturated K_2SO_4	50	10	[14]
ZnO/ZnS@C-750	saturated K_2SO_4	50	11	[15]
Pt-SAs/BNC	saturated K_2SO_4	50	21	[16]
β-PbO_2-120 NRs	PEM	1000	15	[17]
7.7-PtZn/Zn-N-C	saturated K_2SO_4	50	4.2	[18]
Pt/PBDD	PEM	100	29.0	**This work**

11. Reported specific energy consumption for EOP on different anodes.

Table. S5. Reported specific energy consumption for EOP on different anodes

Anode	Cathode	Electrolyte	Power supply	FE (%)	Ec (Wh mg^{-1})	Ref
D10HN410-0.54	Pt mesh	PEM	533 mA cm^{-2}	47	0.143	19
p-BDD-2 min	Stainless steel	PEM	50 mA cm^{-2}	14.3	0.178	20
Nb/BDD-15	Nb	PEM	300 mA cm^{-2}	28.1	0.090	21
Porous PbO2	Pt mesh	PEM	1333 mA cm^{-2}	20	0.065	22
PbO2 nanorod	Pt/C film	PEM	4.0 V	14.0	0.101	11
OFM-Fe-PbO2	Stainless steel	PEM	1.5 A cm^{-2}	10.0	0.250	23
β-PbO2	Stainless steel	PEM	1444 mA cm^{-2}	13.0	0.070	24
Ni/Sb-SnO2	Pt/C	PEM	24.3 mA cm^{-2}	21.4	0.042	25
Ni/Sb-SnO2@3D-PTi	Pt	H-cell	20 mA cm^{-2}	28.0	0.025	4
Pt/PBDD-2	Stainless steel	PEM	100 mA cm^{-2}	29	0.085	This work

D10HN410-0.54: freestanding perforated BDD electrodes, ID was defined from hole diameter (D) and total hole number (HN) as D**HN***.

p-BDD-2 min: a microporous BDD electrode using the technology of oxygen plasma etching.

OFM-Fe-PbO2: Oxide fine-mesh electrodes composed of lead dioxide doped with Fe^{3+}.

12. The Model of Diamond (111) Surface Model.

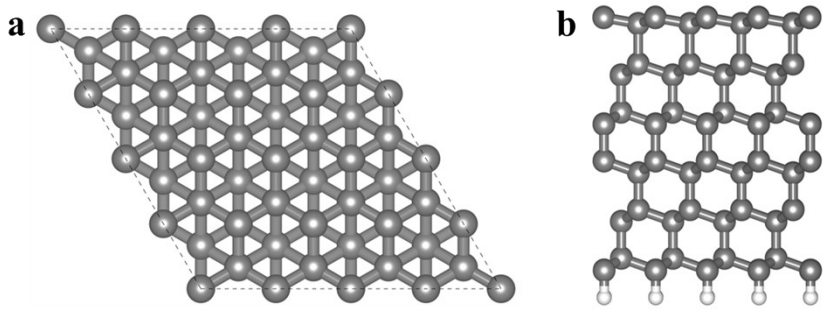

Fig. S8. The top (a) and side (b) views of diamond (111) surface.

13. The conformation of boron-doped diamond.

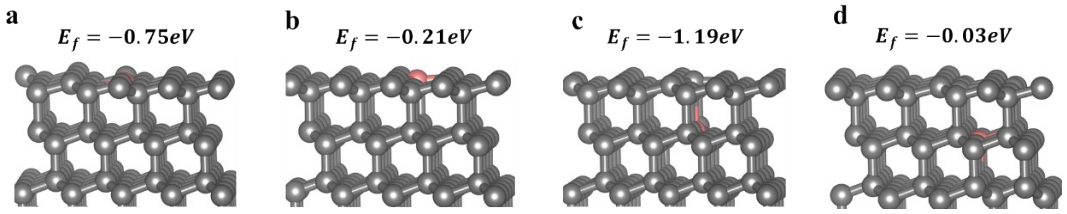

Fig. S9. Relaxation configurations of atom B on surface models located at the first (a), second (b), third (c), and fourth atomic layers from the surface, along with their respective formation energy. Pink spheres correspond to B-doped atoms, while gray spheres represent C atoms.

14. The Free Energy Diagram of the BDD System Reaction Pathway.

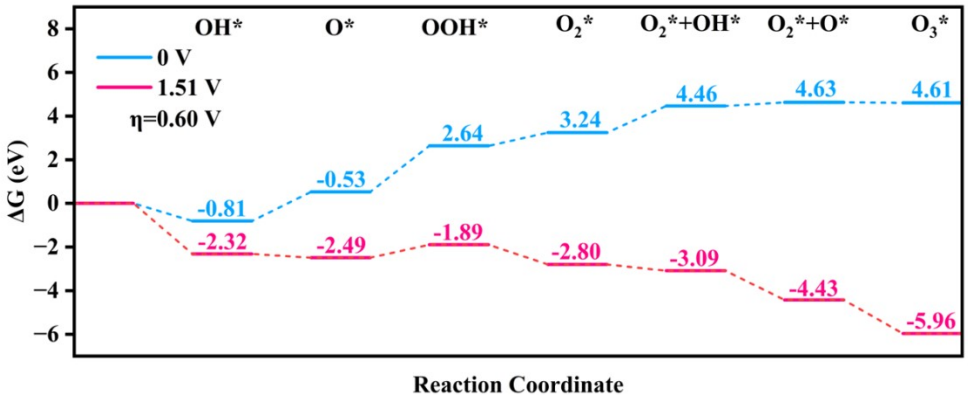

Fig. S10. DFT-calculated free energy diagram (298.15 K) of the proposed reaction pathway on the BDD system.

References

1. M. Hu, D. Zhao, Y. Wang, J. Kang, M. Zhou, H. Q. Fu, B. Johannessen, J. Harbort, J. Harmer, X. Yan, Y. Shu, P. Liu, H. Yin and H. Zhao, *Chin. Chem. Lett.*, 2025, DOI: 10.1016/j.cclet.2025.111192, 111192.
2. F. Gao, X. Li, L. Liu, M. Lu, H. Shi, X. Yu, L. Ding, S. Wang, S. Dai, X. Zhong and J. Wang, *Chem. Eng. Sci.*, 2025, **309**, 121444.
3. Y. Xue, J. Si, J. Cai, Z. Xu, Y. Wang, Y. Wang, M. Xue, Y. Ding, Y. Gu, Y. Cao, S. Wang, H. Cao, X. Zhong and J. Wang, *Chem. Eng. J.*, 2024, **502**, 158098.
4. M. Q. Hu, D. Zhao, M. Y. Dong, H. Q. Fu, Y. Zou, Y. M. Xu, M. Zhou, L. Zhang, L. Wang, Y. J. Shu, K. D. Zhang, Z. Y. Chen, Y. W. Sun, J. Harbort, J. Harmer, P. R. Liu, H. J. Yin and H. J. Zhao, *J Environ Chem Eng*, 2024, **12**, 114915.
5. X. Peng, L. Ding, Z. Bao, J. Liu, H. Shi, X. Wang, X. Zhong, H.-Q. Cao and J. Wang, *Ind. Eng. Chem. Res.*, 2024, **63**, 16312-16323.
6. M. M. Lu, X. Liu, C. F. Jing, X. S. Wang, L. Ding, F. Y. Gao, L. H. Ren, S. Dai, X. Zhong and J. G. Wang, *Adv. Funct. Mater.*, 2025, **35**, 2412170.
7. S.-K. Deng, J.-T. Jiang, T.-L. Tsai, X.-H. Xu and L.-H. Cheng, *Electrochim. Acta*, 2024, **495**, 144390.
8. H. J. Shi, X. S. Wang, X. G. Peng, M. Z. Xue, Y. F. Xue, F. Y. Gao, X. Zhong and J. G. Wang, *J Mater Chem A*, 2024, **12**, 10852-10862.
9. X. Yu, X. Liu, J. Y. Zhao, M. Z. Xue, H. J. Shi, C. H. Jiang, J. Liu, Y. F. Xue, F. Y. Gao, X. Zhong, Z. H. Yao and J. G. Wang, *Chem. Eng. Sci*, 2024, **286**, 119652.
10. H. Shi, G. Feng, T. Sun, X. Wang, L. Ding, Z. Wang, H. Jin, Q. Chen, S. Wang, X. Zhong, Y. Zhu and J. Wang, *Chem Catal.*, 2023, **3**, 100728.
11. X. Wang, D. D. Wu, H. Ge, L. Y. Wang and X. Wu, *J Environ Chem Eng*, 2023, **11**, 110248.
12. X. Wang, J. Li, L. Ding, H. Shi, J. Liu, X. Yang, M. Li, X. Zhong, Z. Yao and J. Wang, *AIChE J.*, 2023, **69**, e18152.
13. J. Liu, C. L. Qiu, Z. X. Xu, M. Z. Xue, J. F. Cai, H. J. Shi, L. Ding, X. N. Li, X. Zhong and J. G. Wang, *Chem. Eng. J.*, 2023, **468**, 143504.
14. X. Yang, W. Li, S. Wang, H. Shi, X. Wang, M. Li, L. Ding, X. Zhong and J. Wang, *ACS EST Engg.*, 2023, **3**, 894-905.
15. L. Ding, J. Zhao, Z. Bao, S. Zhang, H. Shi, J. Liu, G. Wang, X. Peng, X. Zhong and J. Wang, *J Mater Chem A*, 2023, **11**, 3454-3463.
16. Y. Gu, S. B. Wang, H. J. Shi, J. Yang, S. Q. Li, H. Y. Zheng, W. B. Jiang, J. Liu, X. Zhong and J. G. Wang, *Acs Catal*, 2021, **11**, 5438-5451.
17. W. Jiang, S. Wang, J. Liu, H. Zheng, Y. Gu, W. Li, H. Shi, S. Li, X. Zhong and J. Wang, *J Mater Chem A*, 2021, **9**, 9010-9017.
18. B. W. Yuan, Z. H. Yao, C. L. Qiu, H. Y. Zheng, Y. L. Yan, Q. Q. Zhang, X. Sun, Y. Gu, X. Zhong and J. G. Wang, *J Energy Chem*, 2020, **51**, 312-322.
19. K. Arihara, C. Terashima and A. Fujishima, *Journal of The Electrochemical Society*, 2007, **154**, E71.
20. F. Liu, Z. Deng, D. Miao, W. Chen, Y. Wang, K. Zhou, L. Ma and Q. Wei, *J Environ Chem Eng*, 2021, **9**, 106369.
21. X. Lin, H. Q. Liu, B. Wang, W. L. Yang, J. Wang, W. Zhang, W. Yuan, J. Liu, Y. F. Xu and Y. Xiong, *Diam Relat Mater*, 2025, **154**, 112130.

22. S. Stucki, H. Baumann, H. J. Christen and R. Kötz, *Journal of Applied Electrochemistry*, 1987, **17**, 773-778.
23. L. G. De Sousa, D. V. Franco and L. M. Da Silva, *Journal of Environmental Chemical Engineering*, 2016, **4**, 418-427.
24. L. M. Da Silva, D. V. Franco, L. G. Sousa and I. C. Gonçalves, *Journal of Applied Electrochemistry*, 2010, **40**, 855-864.
25. Y. Cui, Y. Wang, B. Wang, H. Zhou, K.-Y. Chan and X.-Y. Li, *Journal of The Electrochemical Society*, 2009, **156**, E75.